Journal of Ceramic Processing Research. Vol. 5, No. 2, pp. 179~186 (2004)

J O U R N A L O F
Ceramic Processing Research

Misorientation distribution of a Mn-Zn ferrite sample with abnormal grain growth

Jong-Sook Lee*

Center for Microstructure Science of Materials and School of Materials Science and Engineering, Seoul National University, Seoul 151-742, Korea

The grain boundary (GB) character of a Mn-Zn ferrite (MZF) specimen exhibiting abnormal grain growth (AGG) was investigated using the electron backscatter diffraction (EBSD) technique. As well as the conventional misorientation angle distribution, the misorientation axis distribution was examined. The distributions were compared to those of the random orientation and geometric criteria for special boundaries of Coincident-Site-Lattice (CSL) and Plane-Matching (PM) models were applied. A close to random misorientation distribution of the AGG microstructure, despite the anisotropy in GB energy, was attributed to the existence of liquid phase arresting further evolution by a solid-state wetting mechanism.

Key words: Mn-Zn Ferrite, electron backscatter diffraction, misorientation distribution, abnormal grain growth.

Introduction

As representative (magnetically) soft ferrites with a wide range of applications, the control of the microstructure is often the crucial part in designing MZF components in order to obtain both high permeability (from the crystal chemistry) and low eddy current losses (from the highly resistive grain boundaries) [1]. In this regard easily occurring AGG in this system has been the subject of investigations either to be prevented or promoted [2-4]. Whatever the phenomenological explanations have been, the microstructures with wavy boundaries and occluded grains appear akin to those of typical secondary recrystallization in metals. The origin of the microstructural evolution in metal systems has been ascribed to the anisotropic GB energy or mobility [5], which is closely related to the grain boundary structure. 'Solid-state wetting' or replacement of high energy GBs by low energy GBs, in analogy to the wetting of GB by liquid phase, has been shown to describe the microstructural evolution appropriately [6, 7].

The EBSD (Electron backscatter diffraction) technique combined with a SEM enables the mapping of crystallographic orientations of large quantities of grains in polycrystalline materials [8]. From the crystallographic orientation of the grains determined by Kikuchi patterns the misorientation between grains are obtained, which correspond to three among the five macroscopic degrees of freedom of GB geometry. Boundaries in ceramic systems are often found wetted by a liquid phase due to the additives and/or impurities. Angular shape grains in the microstructure, if not impinged, are also suggestive of crystals growing from a melt. In the case of a wet boundary, two solid-liquid interfaces exist instead of a GB and the misorientation between two grains becomes irrelevant.

In MZFs, although typically some liquid phase exists in most of the triple junctions as well as at some boundaries [9, 10], low energy 'special' and high energy 'general' GBs lead to low and high barrier effects due to different GB oxidation states [10]. It can be also noted that AGG predominantly occurs when there is little pore dragging [4]. A density inhomogeneity accompanying solid state ceramic processing may be responsible for the frequent initiation of AGG, as also suggested in Ref. [2], when compared to commercial components derived from spray-dried powders. Also glass-forming impurities or additives of Ca and Si were found to hinder AGG [11], by contrast to the usual supposition that AGG in a ceramic system is induced by inhomogeneous distribution of liquid phase. Therefore, a possible link between grain boundary character and microstructural evolution in MZFs is supposed.

We applied the EBSD technique to a MZF specimen in which AGG took place extensively. The misorientation distribution thereby obtained was comprehensively analyzed in comparison with that of a randomly oriented polycrystal and in view of geometric criteria for special low energy boundaries.

*Corresponding author: (at present)
Max-Planck-Institut für Festkörperforschung, Stuttgart, Germany
Tel : +49-711-689-1762
Fax: +49-711-689-1722
E-mail: jong-sook.lee@fkf.mpg.de

Experimental

MZF specimens ($Mn_{0.476}Zn_{0.468}Fe_{2.056}O_4$ by Inductively

Coupled Plasma (ICP) analysis) were prepared by typical ceramic processing: ball-milling, calcining, and sintering (1350 ^{o}C, for 4 hr). No atmospheric control was used. Raw materials were MnCO (Aldrich, 99.9 %), ZnO (Aldrich, 99.99%) and FeO (Kosundo, 99.9%, shape powder ca. 1 μm). A cylindrical compact was cut along the diameter into a flat parallelepiped and polished using diamond pastes. Grain orientations of an overall area of $\sim 1 \times 1$ mm^2 in the microstructure were mapped using an EBSD (electron backscatter diffraction) system (Link opal, Oxford instruments) mounted in a SEM (JEOL 6300). Misorientations between 470 neighboring pairs of grains were identified and individually recorded. Images of mapped neighboring regions were made into a montage to avoid double counting overlapped regions. Lengths of the grain boundaries estimated by the pixel numbers in the digitized image were collated together with the misorientation axis and angle values.

Results

Figure 1(a) shows the microstructure of the specimen prepared in this work as described in Experimental, which is compared with a homogeneous microstructure of a specimen derived from a spray-dried powder of a similar composition [1]. Wavy boundaries and island-like or occluded grains in Fig. 1(a) are characteristic of the microstructure of MZFs with AGG. The optical image reveals mainly etching contrast of grains and grain boundaries so a false impression of extended grains may be given when compared to a skeletonized image of the grains distinguished by EBSD in Fig. 2(a). Figure 2(b) shows a wide and multimodal grain size distribution from 5 μm and 200 μm. The average grain size was estimated to be 57 ± 4 μm.

Figure 3 shows the distribution of misorientation angles of $\sim 1 \times 1$ μm^2 area investigated. The frequency represents the summation of digitally integrated boundary lengths. The distribution of randomly oriented cubic polycrystals [13, 14] is indicated by a solid line as normalized to our experimental distribution. It is uncertain whether or not the differences from the random distribution are significant. According to a chi-square test the distribution is considered random.

Typically, commercial EBSD measurement and analysis packages provide inverse pole figures representing the grain orientations with respect to a laboratory reference frame, which is useful, e.g., for a texture analysis. In Fig. 4 the misorientation axes, not the grain

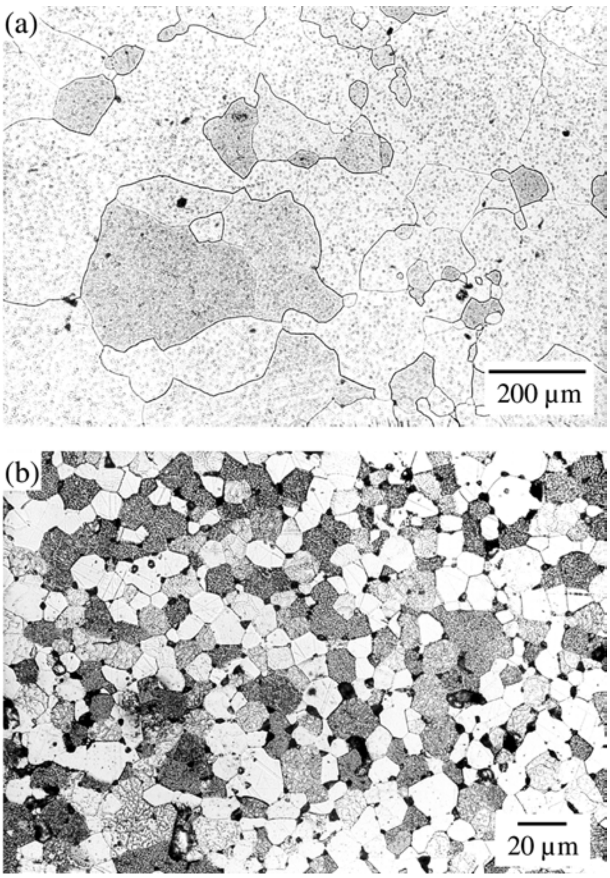

Fig. 1. Micrographs of the MZF specimen with AGG by a conventional laboratory ceramic processing (a) and one with a fine-grained microstructure derived from a spray-dried powder (b).

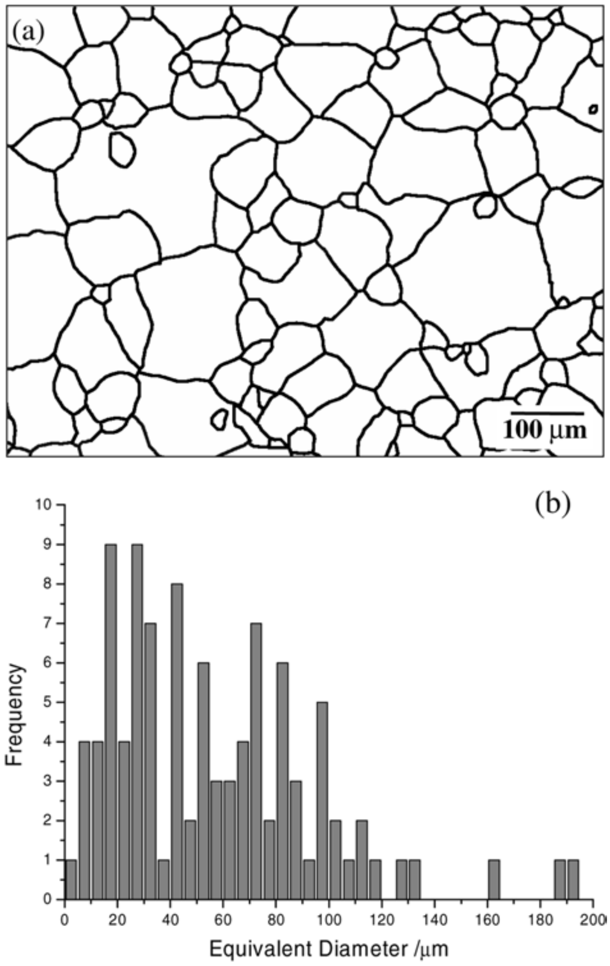

Fig. 2. A skeletonized image representing different grains distinguished by EBSD (a) and the grain size distribution (b).

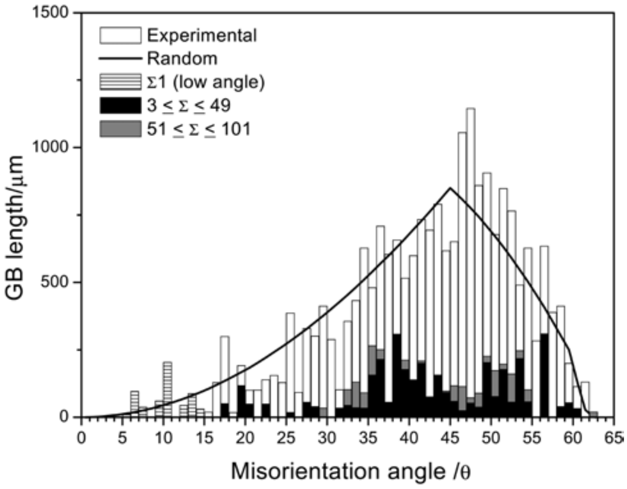

Fig. 3. Misorientation angle distribution of the boundaries. Solid line represent the normalized distribution of the random case. The black portion represents the contribution of the CSL boundaries with $3\leq\Sigma\leq49$ and grey portion with $51\leq\Sigma\leq101$.

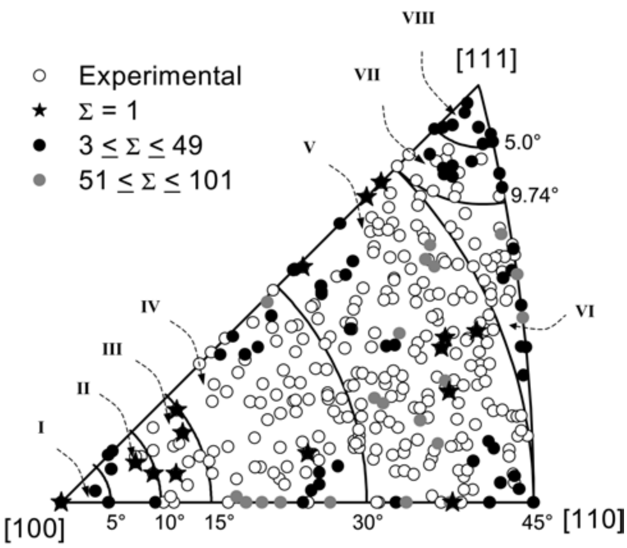

Fig. 4. Inverse pole figure for the misorientation axis distribution. The eight zones according to MacKenzie [17] are designated. The black circles represent the CSL boundaries with $3\leq\Sigma\leq49$ and the grey circles with $51\leq\Sigma\leq101$. The percentages of the boundaries in each zone is shown in Table 1.

orientations, are represented in an inverse pole figure. Randle *et al.* [15, 16] named the representation as Grain-Misorientation-Texture (GMT) distribution. The misorientation axis distribution can be also compared to the random case [17]. The fractions of 8 zones in the stereographic triangle as indicated in Fig. 4 are compared in Table 1. (The zone boundaries are the axes making an angle of 5^o, 10^o, 15^o, 30^o and 45^o, respectively with the [100] axis. The region above 45^o is further divided by the line of 5.0^o and 9.74^o from the [111] axis.) Table 1 shows that the axis distribution, as well as the angle distribution, is also close to random.

An automated CSL analysis based on misorientation data, is a standard feature in an EBSD module. For

Table 1. Axis distribution (in percentages) in comparison with the random case [17]. The zones (I, II, III, etc.) are designated in Fig. 4

	I	II	III	IV	V	VI	VII	VIII
random	0.7	2.1	3.6	22.7	53.4	9.4	6.0	2.1
total	0.53	2.37	2.54	21.18	56.00	8.47	6.38	2.53

CSL statistics a maximum Σ number should be defined. In the literature maximal Σ=29 and 49 have been most frequently used [8], but there is no theoretical justification for these and the cut-off Σ remains rather arbitrary. Some low Σ CSL boundaries have been often found to be 'special', but no direct correlation between the property and Σ numbers exists [18, 19]. On the other hand, there are observations indicating a low energy of boundaries with Σ much higher than 29 or 49 in various materials [20-25]. Therefore Σ up to 101 as listed in Ref. [26] was examined and the result is shown in Fig. 5(a).

For the maximum deviation from an exact CSL relation, the most popular Brandon's criterion, $\Delta\theta_D=15^o\,\Sigma^{-1/2}$ [27], is taken. The maximum deviation angle is then as high as 8.7^o for Σ=3 and 1.5 to 2.1^o for high Σ boundaries over 51. Figure 5(b) represents the deviations of the identified CSL boundaries. It can be seen that many boundaries have deviations close to the limit. The average relative deviation of the CSL boundaries is 0.73. There are also many 'non-CSL' boundaries with deviations slightly above the limit. While an extended upper limit was suggested to be possible [28, 29]. the Brandon's limit is often considered too permissive. More restrictive criteria [30-32] suggested are indicated in Fig. 5(b). According to a more recent Palumbo-Aust criterion, $\Delta\theta_D\leq15^o\,\Sigma^{-5/6}$ [32], only a small number of CSL boundaries are left. In fact, a general expression for the maximum deviation as a function of Σ cannot be given [33]. Moreover, the special properties may decrease in drastic proportion for deviations much smaller than the upper limit $\Delta\theta_M$ of geometric coincidence which is deduced from the existence of GB dislocations [31].

Nevertheless, the Brandon's criterion, owing to its wide usage, is a convenient measure by which the boundary characteristics can be compared with other studies. Garbacz and Grabski [34] estimated the CSL proportions for $\Sigma\leq65$ in a randomly oriented crystal. Their results are compared with the experimental results of this study in Fig. 6 for cut-off Σ=49. A random crystal has 12.9% of boundaries with $3\leq\Sigma\leq49$ while the MZF specimen in this work has somewhat higher proportion as 16.0%. Black portions of the columns in the misorientation angle distribution in Fig. 3 represent the angle distribution of these boundaries whereas their misorientation axes are indicated in Fig. 4 by black circles.

Besides the difference in the overall percentages, the

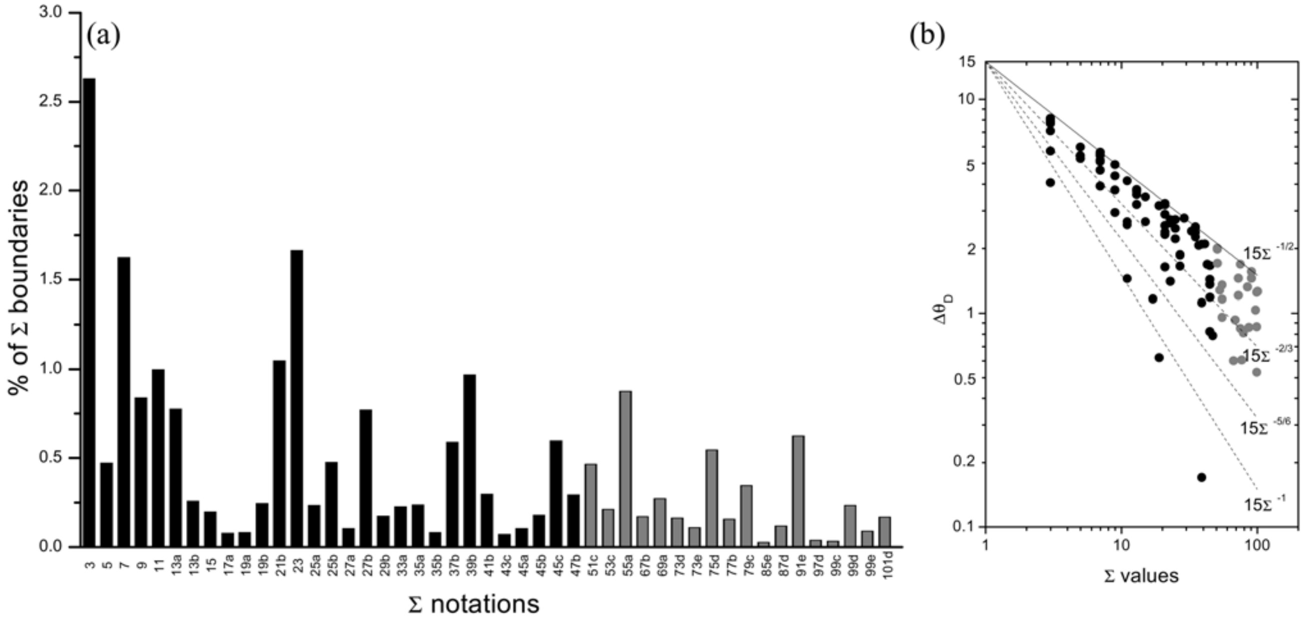

Fig. 5. (a) Distribution of the CSL boundaries with 3≤Σ≤101. (b) Deviation angles from exact CSL misorientations according to the Brandon's criterion. Other more restrictive criteria are also shown.

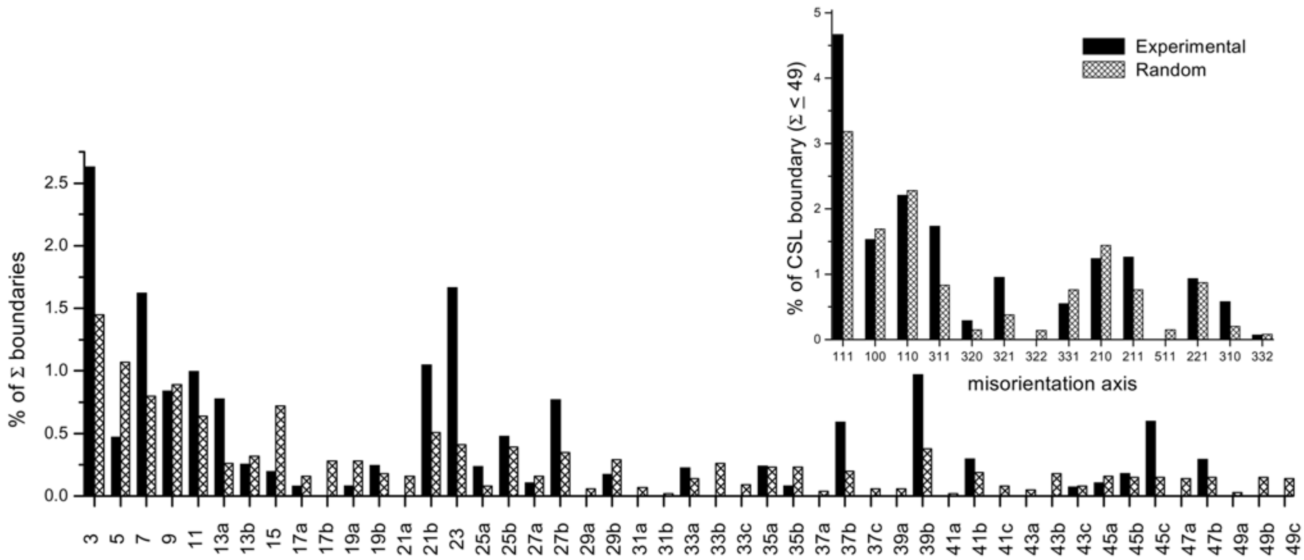

Fig. 6. Distribution of the CSL boundaries (3≤Σ≤49) in comparison with the random case [34]. The inset shows the proportions with respect to the associated CSL rotation axis.

proportions of the respective Σ boundaries were found to be at pronounced variance with the random case, as can be seen in Fig. 6. CSL boundaries such as Σ=3, 7, 13a, 21b, 23, 27b, 37b, 39b and 45c exhibit higher fractions than in random case, while the boundaries with Σ=5, 15, 17a, 17b, 19a, 21a, 33b, 35b, 43b, 47a, 49b, and 49c, indicate a smaller presence. Preference of certain Σ boundaries appears to be partly related to the preference of certain CSL misorientation axes. CSL boundaries with the axes of [111], [311], [321], [211], and [310] exhibit higher proportions than in the random case as shown in the inset of Fig. 6.

The CSL boundaries with Σ ≥ 51 were found to constitute 4.5% of the total boundary length as represented by grey portions in angle distribution in Fig. 3. Grey circles in Fig. 4 indicate their axes. Figure 5(a) shows that high Σ boundaries of 51c, 55a, 75d, and 91e are as much present as with low Σ numbers of 5, 9, 11 and 13a. Star symbols in Fig. 4 represent the axes of the low angle boundaries ($\theta \leq 15^o$) or Σ=1, as shaded in Fig. 3. (Although some high Σ misorientations are associated with low angle values [26], they were not found in the region investigated of this study. Some boundaries with angles lower than 5^o may have been overlooked in the data collection due to the small difference in colors indicating orientations.) Including

Σ=1, the entire CSL proportion ≤101 amounts to 23.2 %. The CSL boundary fraction for a commercial fine-grained MZF specimen was reported >15% [35] and >10% [10], but the cut-off Σ values in their estimations were not given.

It should be noted that the CSL boundaries in the present analysis and in most other EBSD studies are designated based on the misorientation information alone. The misorientation angle and axis are only three parameters among the five degrees of freedom for describing the (macroscopic) geometry of a boundary. Boundary plane orientation or inclination corresponding to the other two degrees of freedom is not known. (Some studies have attempted EBSD investigations based on serial sections of the microstructure to determine the grain-boundary planes [36, 37].) In the CSL model the boundary planes with a high coincidence account for the low energy of the boundary [38]. For example, Σ=3 and Σ=11 misorientation boundaries exhibit a deep energy cusp [39, 40], only when they are symmetric tilt grain boundaries with boundary planes of (111) and (311), respectively. In this sense, CSL boundaries mentioned in this work are more properly 'CSL misorientation' boundaries.

On the other hand, the misorientation axis alone is a criterion for GB energy according to Plane Matching (PM) model [41-43]. The Coincident Axis Deviation (CAD) or PM model prescribes that a high angle GB across which a single set of low index planes is continuous, e.g. with a [111] misorientation axis, is one of low energy, regardless of the misorientation angles. By contrast, the CSL model specifies certain misorientation angles for a given misorientation axis, viz., for [111] rotation axis, 60^o(Σ=3), 38.21^o(Σ=7), 27.89^o(Σ=13b), etc. are considered special. A more suitable terminology for CSL and PM boundaries are three-dimensional coincidence and one-dimensional coincidence GB [44] and a PM boundary can be regarded as the limiting case of a CSL boundary with Σ going to ∞ [45]. In the PM model boundary planes do not play a role.

GB dislocations suggesting PM boundaries have been detected for boundaries with respect to the low index axes of [111], [100], and [110] over a considerable range of deviation as 20^o [46, 47]. There is so far no accepted definition with regard to the maximum deviation for PM boundaries, although a criterion analogous to the Brandon limit for CSL boundaries was suggested [48]. We examined the distributions of the misorientation axes around low index axes. Figure 7 displays some contours of a fixed deviation θ from the low index axes in an inverse pole figure. (Contours of 5^o and 10^o deviation from [100] and 5^o deviation from [111] coincide the zone boundaries indicated in Fig. 4.) Percentages of the boundaries within deviations (θ) of 3^o, 5^o, 7.5^o, 10^o, and 15^o are estimated in Table 2. For a randomly oriented polycrystal the probability density on the axes [100], [111] and [110] is 2.285, 5.287, and 5.473, respectively, and the relative proportions of axes lying within a small angle θ of the respective axes are approximately 1:3.1:4.8 [17]. The relative proportions of the axes [100] and [111] (1:3.1) hold approximately up to 10^o in the random case, Table 1, so did our experimental results, Table 2. Since the probability density drastically varies from [110] in the radial directions as well as with θ (See Fig. 1 in Ref. [17]), the approximate relative proportions of the axis [110] should be valid only for a small θ. In this regard the proportion within 3^o of [110] relative to that of [100] appears to fit the random case but boundaries concerned in this range are rather few.

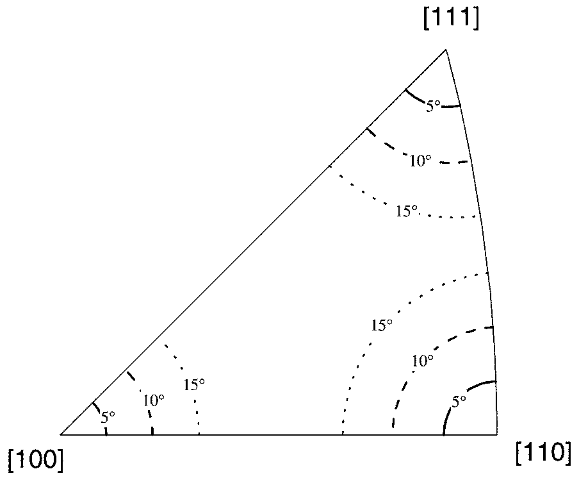

Fig. 7. Contours of deviations of 5^o, 10^o, and 15^o from the low index axes in an inverse pole figure.

Table 2. The percentages of the boundaries with misorientation axes within an angle (θ) of the axes of low indices, [111], [100] and [110]

θ	111	100	110
3.0^o	0.47	0.22	1.10
5.0^o	2.54	0.53	1.94
7.5^o	4.89	1.45	5.46
10.0^o	8.91	2.90	10.56
15.0^o	18.84	5.44	21.61

Some TEM observations on the present MZF specimen have been also made. Figure 8(a) shows an island-like grain of a size close to the limit detected by EBSD. A higher magnification of a segment in Fig. 8(b) shows diverse features depending on inclinations: Flat regions of ~100 nm of different orientations (as indicated), a hill-and-valley structure (top left) and a curved portion (bottom) exist. If there is no amorphous phase present at the boundary and if the boundary is in an equilibrium structure, the features represent the GB Wulff shape for the given misorientation of the island grain with respect to the matrix [49].

Figure 8(c) shows a TEM image of a triple junction with a glassy second phase. Similar to Fig. 8(b) the solid-liquid interface of a grain (A) exhibits both faceted

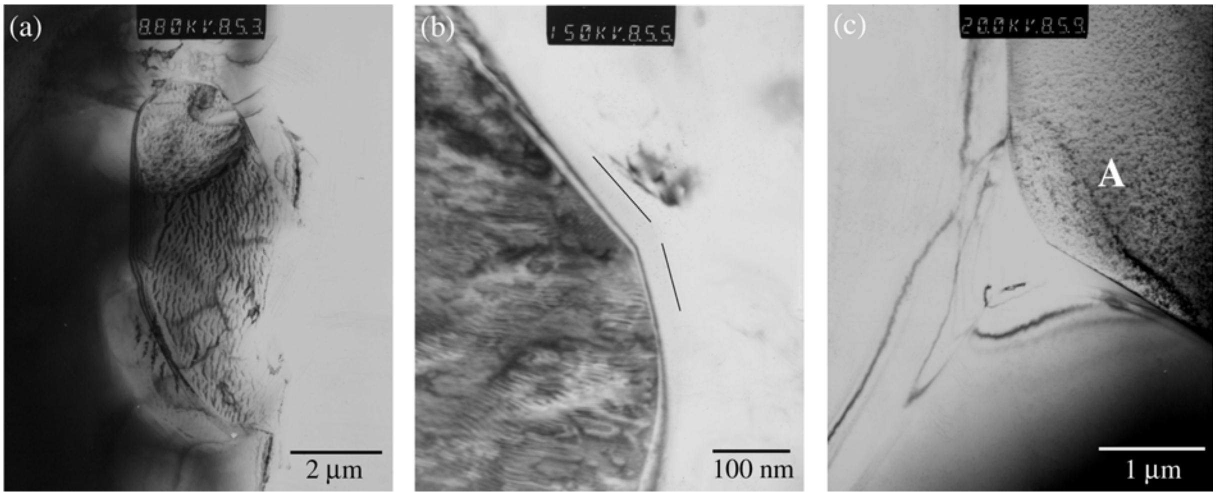

Fig. 8. (a) TEM micrograph of an island grain. (b) Boundary segment of the island grain exhibiting flat and hill-and-valley facets and also a curved region on a higher magnification. (c) Triple junction containing a liquid phase. Faceted and curved interface of the grain **A** can be observed.

and curved shape. The liquid phase appears to penetrate along the GB with the faceted interface. TEM-EDS (Energy Dispersive X-Ray Spectrometry) showed that the liquid phase at the triple junctions contains a significant phosphorous content as well as Ca and Si. Phosphorous as an impurity had been reported to promote grain growth in MZF [50].

Discussion

The analysis (Fig. 3, Fig. 4 and Table 1) showed that misorientation distribution of the investigated MZF specimen with AGG is not significantly different from that of a random oriented polycrystal. The CSL distribution suggested a non-random character, nevertheless (Fig. 6).

The existence of GB energy anisotropy of the material has been indicated by another investigation [51]: When the boundaries were grouped into a high-resistance and low-resistance set, based on microcontact impedance measurements on the individual boundaries [51, 52], significantly different misorientation distribution emerged. The CSL analysis was not particularly useful in accounting for this difference. The overall proportion of the CSL misorientation boundaries was found only slightly higher (by 10%) in the low resistance group than in the high resistance group. The CSL distributions differed notably, but the comparison suffered from the scarcity of observations. Notable was that all the electrically probed four Σ=21b (44.4^o, [211]) and three Σ=23 (40.5^o, [311]) boundaries belong to the low resistance group (with one of them shared also by the high-resistance group), since they are also preferred CSL boundaries in the overall distribution in comparison with the random case, as shown in Fig. 6.

Comparison of the misorientation axis distribution according to the PM model allowed a more definite statement: 12% of the low resistance group exists within a 10^o deviation from the [110] whereas only 5% of the high resistance group is located in the same region. Besides, the axes between [111] and [100] axes (such as [433], [755], [533], [211], [311] and [411]) or near the 15^o contour of the [111] axis were found relatively preferred in the low resistance group. Although the physics behind the specialty of PM type boundaries seems not well understood [46], there have been reports suggesting the importance of the misorientation axis in the determination of the boundary energy in various materials [25, 53-55]

Misorientation approaches facilitated by EBSD are subject to the criticism for disregarding the microscopic details of the interface, first of all, the grain boundary plane information. Faceting of the boundaries as in Fig. 8(b) represents the dependence of GB energy on the boundary orientation (when the boundary is in an equilibrium structure). Recent progress in theoretical and experimental studies reveals the diversity and multiplicity of GB structures, which is not covered by simple geometric criteria such as CSL theory. Asymmetric boundaries of a comparatively low as or even a lower energy than the symmetric boundaries have been found to exist in a number of configurations and they are considered to be a significant part of randomly inclined boundaries of space-filling grains in a polycrystal [56, 57]. Asymmetric boundaries have been observed for high Σ misorientation as well as low Σ boundaries [25, 56, 57]. The preference of asymmetric boundaries has been attributed to the densely packed boundary plane(s) [57, 58]. The limitation of this criterion was discussed by Sutton and Balluffi [18, 49]. According to Paidar [59, 60] not the single parameter of the interplanar spacing, but the distribution of interplanar spacings which contains the information on the misorientation of two grains should be considered, since it puts together the inclination of the boundary plane and the rotation of the grains. A purely geometrical classification scheme of the interface was thus derived, which is compatible with a structural unit model based on systematic computer calculations using different atomic potentials [61]. Sutton and Vitek showed that the structures of GBs with a fixed rotation axis are composed, in a certain range of misorientation angles, of various combinations of two structural units out of which the boundaries defining the misorientation range are built. Padier extended his classification scheme to non-periodic (non-CSL) asymmetric tilt boundaries [62]. The model thus connects the misorientation distribution and boundary plane orientation, which are actually independent parameters for the boundary geometry. In fact, the misorientation angles of the [110]-type PM (non-CSL) boundaries of the low resistance group [51] was found to coincide with some of the asymmetrical configurations with densely packed planes of the f.c.c. structure, {111}, {100}, {311} and {331} [62]. Further links between boundary plane configurations and the misorientations may be found, when the misorientations in the minimum-angle notation used in this work are re-examined in other equivalent rotations with a low-index rotation axis of interest as in Ref. [25, 54, 62].

According to solid state wetting mechanism [7], the AGG microstructure of MZFs should be eventually dominated by low energy GBs, the character of which has been above introduced. However, the misorientation distribution of the overall microstructure with extensive AGG was found to be rather characterless and close to random as shown in Fig. 3 and Table 1. The results should not be considered to exclude any role of GB structure in the microstructural evolution of MZFs. It is supposed that an averaged-out random distribution has resulted as locally initiated AGG regions collided with each other in a random manner. The existence of wet boundaries and the liquid-filled triple pockets as shown in Fig. 8(c) are considered to prevent further evolution driven by the GB energy anisotropy, i.e. solid-state wetting along grain boundaries or triple junctions [7]. The supposition can be proved when the microstructure with isolated AGG regions is investigated and the preliminary results appear positive. The role of the liquid-phase enhanced grain growth by solution-reprecipitation process is not excluded [63]. The interplay between GBs and wetted boundaries in microstructural evolution is considered an important research subject in ceramic systems.

Summary

MZF specimens prepared by a conventional solid state route exhibited AGG extensively. Misorientations of 470 GBs over ~1×1 mm^2 were obtained by EBSD in a SEM. When compared to a randomly oriented crystal, misorientation axis and angle distributions of the MZF specimen appeared close to random. The CSL distribution was found different from the random case and the overall proportion was higher (16% vs. 12% for $3 \leq \Sigma \leq 49$). The reason why the character of the low energy GBs, evidenced in other report, did not dominate the microstructure is suggested to be the arrested microstructural evolution by solid-state wetting due to the existence of the liquid phase.

Acknowledgement

This work was supported by Creative Research Initiatives of the Korean Ministry of Science and Technology.

References

1. G. Alex, “Modern Ferrite Technology” (Van Nostrand Reinhold, New York, 1990).
2. G.R. Chol, J. Am. Ceram. Soc. 54[1] (1971) 34-39.
3. M. Drofenik, S. Beseničar, M. Limpel, and V. Gardaševič, in Advances in Ceramics Vol. 16, edited by F.F. Wang (American Ceramic Society, Columbus, OH, 1985) p. 229.
4. A. Ikeda, M. Satomi, H. Chiba, and E. Hirota, in “Ferrites”, edited by Y. Hoshino, S. Lida, and M. Sugimoto (University Park Press, Baltimore, MD, 1971) p. 337.
5. A.D. Rollett, D.J. Srolovitz, and M.P. Anderson, Acta Metall. 37[4] (1989) 1227-1240.
6. N.M. Hwang, J. Mater. Sci. 33 (1998) 5625-5629.
7. N.M. Hwang, S.-B. Lee, and D.-Y. Kim, Scr. Mater. 44 (2001) 1153-1160.
8. V. Randle, “The Role of the Coincidence Site Lattice in Grain Boundary Engineering” (The Institute of Materials, London, 1996).
9. P.E.C. Franken and W.T. Stacy, J. Am. Ceram. Soc. 63[5-6] (1980) 315-319.
10. J.-Y. Laval, C. Cabanel, M.-H. Berger, and P. Girard, J. Am. Ceram. Soc. 81[5] (1998) 1133-1140.
11. Y.S. Cho, D. Schaffer, V.L. Burdick, and V.R.W. Amarakoon, Mater. Res. Bull. 34[14/15] (1999) 2361-2368.
12. S.C. Byeon, K.S. Hong, J.G. Park, and W.N. Kang, J. Appl. Phys. 81[12] (1997) 7835-7841.
13. J.K. Mackenzie, Biometrika 45[1-2] (1958) 229-240.
14. A. Morawiec, J. Appl. Cryst. 28 (1995) 289-293.
15. V. Randle and B. Ralph, Proc. R. Soc. Lond. A 415 (1988) 239-256.
16. V. Randle, “The Measurement of Grain Boundary Geometry” (IOP Publishing Ltd, 1993).
17. J.K. Mackenzie, Acta Metall. 12[2] (1964) 223-225.
18. A.P. Sutton and R.W. Balluffi, Acta Metall. 35[9] (1987) 2177-2201.
19. P.J. Goodhew, in “Grain Boundary Structures and Kinetics,” edited by R.W. Balluffi (American Society for Metals, Metals Park, OH, 1980) p. 155.
20. L.S. Shvindleman and B.B. Straumal, Acta Metall. 33[9] (1985) 1735-1749.
21. B. Loberg and H. Nordén, Acta Metall. 21[3] (1973) 213-218.
22. P.J. Goodhew, T.Y. Tana, and R.W. Balluffi, Acta Metall. 26[4] (1978) 557-567.
23. H. Mykura, P.S. Bansal, and M.H. Lewis, Philos. Mag. A 42[2] (1980) 225-233.
24. G. Herrmann, H. Gleiter, and G. Bäro, Acta Metall. 24 (1976) 353-359.

25. C.B. Carter, Acta Metall. 36[10] (1988) 2753-2760.
26. H. Mykura, in “Grain-Boundary Structure and Kinetics” edited by R.W. Balluffi (American Society for Metals, Metals Park, OH, 1980) p. 445.
27. D.G. Brandon, Acta Metall. 14[11] (1966) 1479-1484.
28. R.W. Balluffi and T.Y. Tan, Scr. Metall. 6[11] (1972) 1033-1040.
29. G.L. Bleris, J.G. Antonopoulous, T. Karakostas, and P. Delavignette, Phys. Status Solidi (a) 67[1] (1981) 249-257.
30. Y. Ishida and M. McLean, Philos. Mag. 27 (1973) 1125-1134.
31. M. Déchamps, F. Baribier, and A. Marrouche, Acta Metall. 35[1] (1987) 101-107.
32. G. Palumbo and K.T. Aust, Acta Metall. 38[11] (1990) 2343-2352.
33. P.H. Pumphrey, in “Grain Boundary Structure and Properties,” edited by G.A. Chadwick and D.A. Smith (Academic Press, New York, 1976) p. 139.
34. A. Garbacz and M.W. Grabski, Scr. Metall. 23 (1989) 1369-1374.
35. J.J. Pinet-Berger and J.Y. Laval, in “Ceramic Microstructure ´86,” edited by J.A. Pask and A.G. Evans (Plenum Press, 1987) p.657.
36. V. Randle, J. Mater. Sci. 30[16] (1995) 3983-3988.
37. D.M. Saylor, A. Morawiec, and G.S. Rohrer, J. Am. Ceram. Soc. 85[12] (2002) 3081-3083.
38. D.G. Brandon, B. Ralph, S. Ranganathan, and M. Wald, Acta Metall. 12[7] (1964) 813-821.
39. G.C. Hasson and C. Goux, Scr. Metall. 5[10] (1971) 889-894.
40. M. McLean, J. Mater. Sci. 8 (1973) 571-576.
41. P.H. Pumphrey, Scr. Metall. 6[2] (1972) 107-114.
42. P.H. Pumphrey, Scr. Metall. 7[9] (1973) 893-897.
43. B. Ralph, P.R. Howell, and T.F. Page, Phys. Status Solidi (b) 55[2] (1973) 641-652.
44. L. Priester, Revue Phys. Appl. 24[4] (1989) 419-438.
45. D.H. Warrington and H. Grimmer, Philos. Mag. 30[3] (1974) 461-468.
46. R. Schindler, J.E. Clemans, and R.W. Balluffi, Phys. Status Solidi (a) 56[2] (1979) 749-761.
47. J. Levy, Phys. Status Solidi 31[1] (1969) 193-201.
48. D.H. Warrington and M. Boon, Acta Metall. 23[5] (1975) 599-607.
49. A.P. Sutton and R.W. Balluffi, “Interfaces in Crystalline Materials” (Clarendon Press, Oxford, 1995).
50. S. Otobe, T. Hashimoto, H. Takei, and T. Maeda, J. Phys. IV France 7[C1] (1997) 127-128.
51. J.-S. Lee, D.-Y. Kim, J. Fleig, and J. Maier, J. Am. Ceram. Soc. to be published.
52. J.-S. Lee, J. Fleig, J. Maier, and D.-Y. Kim, J. Mater. Res. 19[3] (2004) 864-871.
53. Y. Ishida and T. Yamamoto, T. Jpn. I. Met. 18[3] (1977) 221-231.
54. W. Lojkowski, H. Gleiter, and R. Maurer, Acta Metall. 36[1] (1988) 69-79.
55. Y. Zhu, H. Zhang, H. Wang, and M. Suenaga, J. Mater. Res. 6[12] (1991) 2507-2518.
56. K.L. Merkle and D. Wolf, Philos. Mag. A 65[2] (1992) 513-530.
57. D. Wolf and K.L. Merkle, in “Materials Interfaces: Atomic-Level Structure and Properties,” edited by D. Wolf and S. Yip (Chapman & Hall, 1992) p. 87.
58. D. Wolf, J. Phys. C4 46 (1985) 197-210.
59. V. Paidar, Phys. Status Solidi (a) 92 (1985) 115-120.
60. V. Paidar, Acta Metall. 35[8] (1987) 2035-2048.
61. A.P. Sutton and V.Vitek, Philos. T. Roy. Soc. A 309[1509] (1983) 1-68.
62. V. Paidar, Philos. Mag. A 66[1] (1992) 41-54.
63. M. Drofenik, A. Žnidarš, and D. Makovec, J. Am. Ceram. Soc. 86[9] (2003) 1601-1604.